Elliottite, $NaMgAl_3(PO_4)_2F_6 \cdot 9H_2O$; a new crandallite-derivative mineral from Tom's phosphate quarry, Kapunda, South Australia

Ian E Grey[1*], W Gus Mumme[1], Colin M MacRae[1], Anthony R Kampf[2] and Stuart J Mills[3]

Abstract

Elliottite, $NaMgAl_3(PO_4)_2F_6 \cdot 9H_2O$, a new secondary phosphate mineral, is from Tom's phosphate quarry, Kapunda, South Australia. It occurs as hemispherical aggregates to 1 mm across comprising pseudohexagonal platelets overgrowing minyulite and amorphous angastonite on a matrix of goethite. Closely associated minerals are penriceite and wavellite. The calculated density is 2.09 $g \cdot cm^{-3}$. Optically the crystals are biaxial (+) with $\alpha = \beta = 1.475(2)$, $\gamma = 1.479(2)$, 2V(calc) = 0°, orientation is $Z \approx \mathbf{c}$. There is no birefringence evident when viewing normal to the plates and the crystals display strong pseudo-uniaxial optical behaviour. Electron microprobe analyses give an empirical formula based on 23 anions of $Na_{0.56}K_{0.40}Ca_{0.02}Mg_{1.79}Al_{2.27}P_{2.02}F_{4.33}H_{20.19}O_{18.67}$. Elliottite is monoclinic, space group $C2/m$ (#12), with a = 12.242(1) Å, b = 7.0118(7) Å, c = 11.2946(9) Å, β = 101.19(1)°, V = 951.1(2) $Å^3$ and Z = 2. The crystal structure was determined from an analysis of powder X-ray diffraction data. It represents a new type of crandallite-derivative layer structure, with the same topology of corner-connected aluminium-centred octahedra and PO_4 tetrahedra as in crandallite, but with an expanded layer separation due to the location of $Mg_2(H_2O)_{10}$ edge-shared octahedral dimers and water molecules in the interlayer region. Elliottite and penriceite have the same ideal formula and so are dimorphs: the structure of penriceite can be described as being derived from that of elliottite by periodic unit-cell-scale twinning.

KEYWORDS: elliottite, penriceite, Tom's phosphate quarry, Kapunda, South Australia

Introduction

Tom's phosphate quarry, near Kapunda in the Koonunga Hill area, South Australia, is an openpit mine that exploits phosphorite-type rock phosphate to produce phosphate fertilizer. Mining of the deposit began soon after its discovery in 1904 and continues to the present day. As reported by Elliott et al. (2013) the phosphate rock is distributed throughout calcareous clay derived from the decomposition of argillaceous rocks underlying the Kapunda Marble formation. The phosphorite has a high iron content that limits its use in superphosphate production but made it an attractive feedstock for high-phosphorus pig-iron production during the Second World War.

Its ready accessibility has made Tom's quarry a mecca for mineral collectors and mindat.org (www.mindat.org, accessed 14/4/2022) records 64 valid mineral species being identified in specimens from the quarry, including three secondary phosphate minerals for which Tom's quarry is the type locality. These are peisleyite, $Na_2Al_9[(P,S)O_4]_8(OH)_6 \cdot 28H_2O$ (Pilkington et al., 1982; Mills et al., 2011), kapundaite, $(Na,Ca)_2Fe^{3+}_4(PO_4)_4(OH)_3 \cdot 5H_2O$ (Mills et al., 2010) and jahnsite-(CaFeMg), $CaFe^{2+}Mg_2Fe^{3+}_2(PO_4)_4(OH)_2 \cdot 8H_2O$ (Elliott, 2016). Elliottite, $NaMgAl_3(PO_4)_2F_6 \cdot 9H_2O$, is the fourth new phosphate mineral to be described from the locality. It has been formally approved as a new species by the IMA Commission on New Minerals, Nomenclature and Classification (2021-113). The name is for Peter Elliott (born Adelaide, 17 November 1954) in recognition of his significant contributions to the characterization and naming of more than 30 new minerals from Australian localities (half of which he personally collected) and in particular his major contributions to the descriptions of new phosphate minerals from South Australian deposits. These include airdite, bimbowrieite, penriceite, plumboperloffite, puttapaite, reaphookhillite, whiteite-(MnMnMg) and whiterockite. He is first author on a review of the phosphate deposits of South Australia (Elliott et al., 2013). The holotype specimen of elliottite is housed in the mineralogical collections of the Museum of South Australia, catalogue number G35026. A sub-sample of the holotype specimen, used for optical measurements, is in the collections of the Natural History Museum of Los Angeles County, catalogue number 76203. Co-type specimen M45575 is a portion of the type specimen for angastonite, housed at Museums Victoria.

Occurrence and paragenesis

The type locality for elliottite is Tom's phosphate quarry (34°21'33"S, 138°59'17"E), 7 km southeast of Kapunda, South Australia (Fig. 1). The holotype specimen is a small hand specimen measuring 2 cm × 1 cm (Fig. 2). It comprises hemispherical aggregates to 1 mm across of platy crystals of elliottite, overgrowing minyulite on a matrix of goethite. Other closely associated minerals are penriceite and wavellite. Elliottite is also the dominant mineral (by powder X-ray diffraction) in the angastonite type specimen number M45575 (Museums Victoria specimen) from the Penrice marble quarry, located about 15 km southeast of Tom's quarry. At Penrice, elliottite is associated with

1 CSIRO Mineral Resources, Private Bag 10, Clayton South, VIC 3169, Australia

2 Mineral Sciences Department, Natural History Museum of Los Angeles County, 900 Exposition Boulevard, Los Angeles, CA90007, USA

3 Geosciences, Museums Victoria, GPO Box 666, Melbourne, VIC 3001, Australia

* Corresponding author: ian.grey@csiro.au

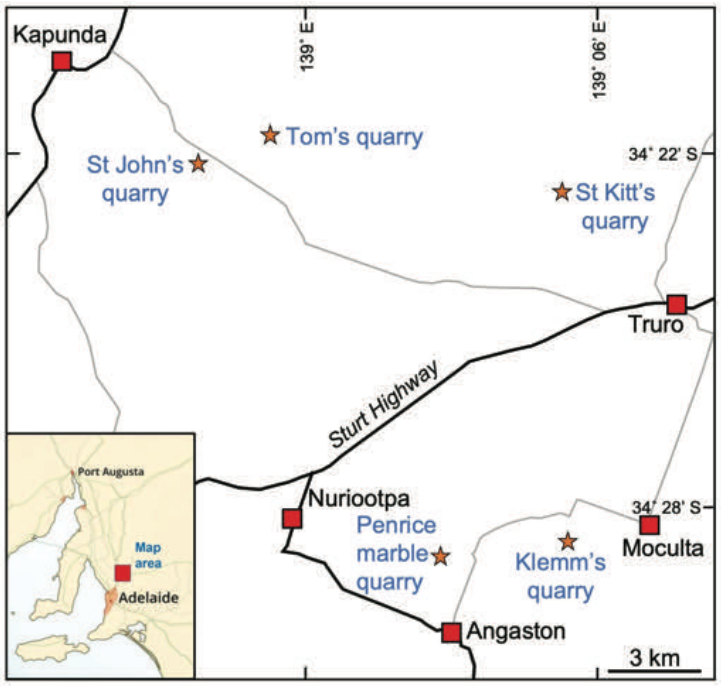

Figure 1 **Location of the Kapunda–Angaston phosphate deposits.**

crandallite, minyulite, penriceite, perhamite, quartz and an amorphous calcium–magnesium–aluminium phosphate that has the composition reported for angastonite (Mills et al., 2008). Recently, angastonite has been redefined as an amorphous mineral (Grey et al. 2022a). The formation of elliottite is related to the alteration of minyulite, $KAl_2(PO_4)_2F{\cdot}4H_2O$ (Grey et al., 2022b), in near-neutral solution. Potassium and fluorine are leached and the leach product takes up solution species Mg^{2+}, Ca^{2+} and Na^{+} to form amorphous angastonite, which subsequently crystallizes as elliottite and penriceite. Whereas penriceite platelets grow outwards from the surface of the amorphous phase, the elliottite platelets form within the amorphous/residual minyulite matrix (Fig. 3).

Appearance and properties

Elliottite occurs as ultra-thin pseudohexagonal platelets, typically 50 to 100 μm in diameter (Figs 3–5). The platelets are less elongated than the pseudohexagonal platelets of associated penriceite. They are colourless with a white streak and have perfect cleavage on {001}. The calculated density is 2.09 $g{\cdot}cm^{-3}$ for the empirical formula.

Figure 2 **Elliottite aggregates of platelets on goethite matrix, South Australian Museum specimen G35026. Field of view is 2 mm wide. Photo Peter Elliott.**

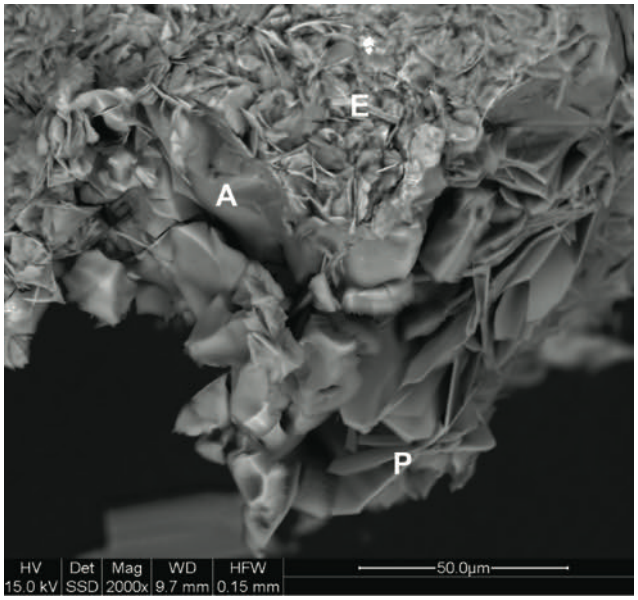

Figure 3 Scanning electron microscope (SEM) image showing platelets of penriceite (P) on the lower surface of an anhedral amorphous angastonite (A) matrix containing very small platelets of elliottite (E).

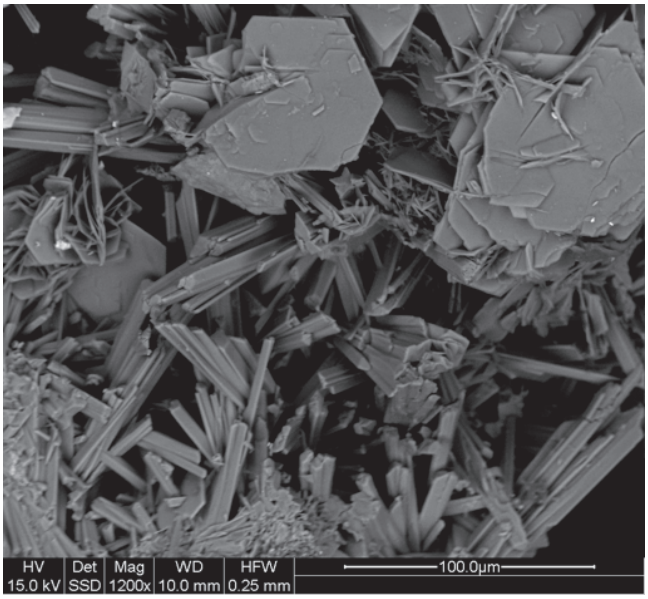

Figure 4 Back-scattered electron image of pseudohexagonal elliottite platelets (upper half) associated with wavellite rods (lower half) in specimen G35026.

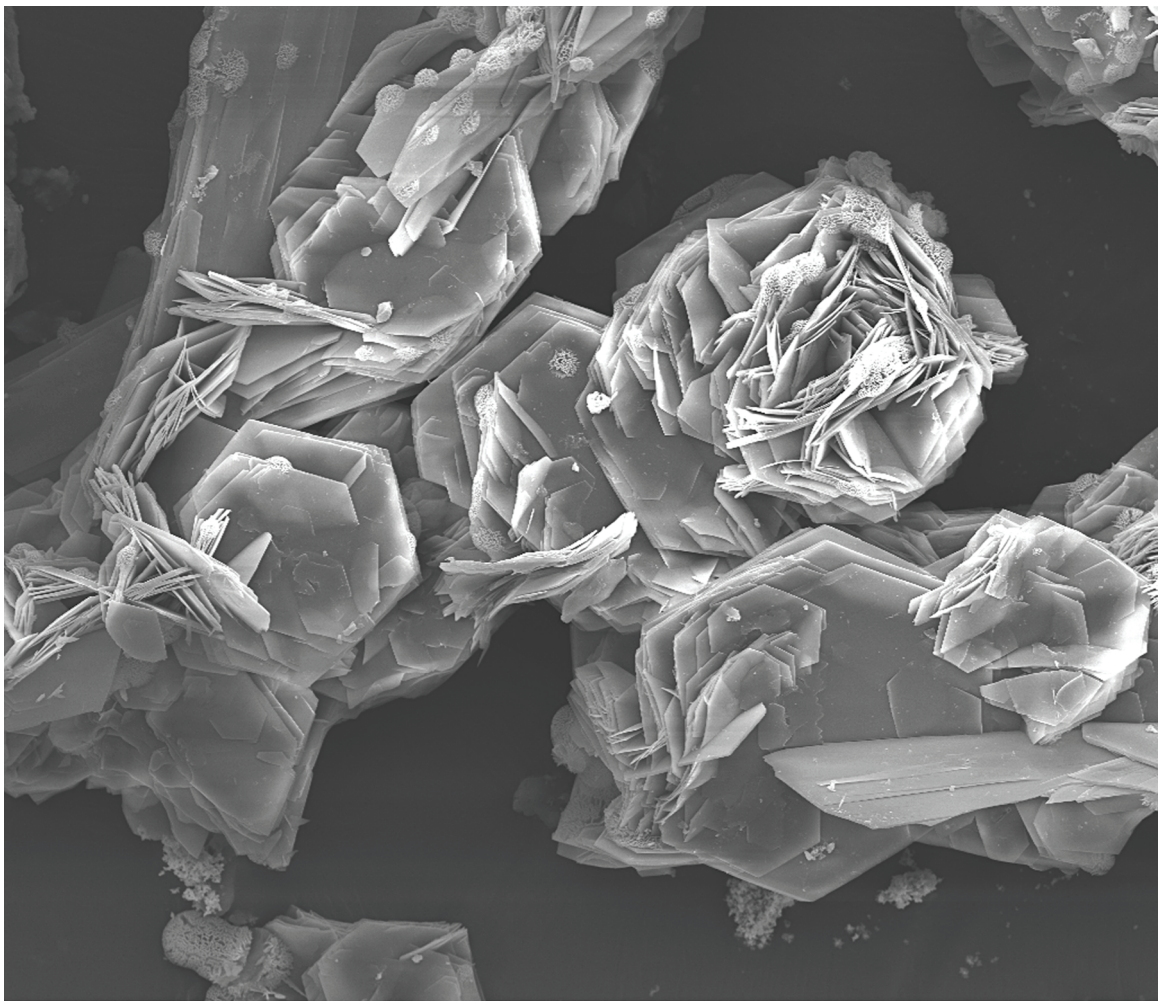

Figure 5 SEM image of pseudohexagonal elliottite platelets from the Penrice marble quarry. Field of view is 0.25 mm wide. Image Peter Elliott.

Elliottite crystals are biaxial (+), but strongly pseudo-uniaxial, with $\alpha = \beta = 1.475(2)$, $\gamma = 1.479(2)$ (white light). The calculated 2V is 0°. The orientation is $Z \approx \mathbf{c}$. No dispersion or pleochroism was observed. There was no birefringence evident when viewing normal to the platelets. The Gladstone-Dale compatibility index (Mandarino, 1981) $1-(K_P/K_C) = -0.044$ (good), based on the empirical formula and PXRD unit-cell parameters for G35026.

Infrared spectroscopy

The infrared spectrum of specimen G35026 of elliottite (Fig. 6) was obtained on ground crystals using a Nicolet 5700 FTIR spectrometer (range 700 to 4000 cm^{-1}) equipped with a Nicolet Continuum IR microscope and a diamond-anvil cell. A broad band is observed in the OH-stretching region centred at 3300 cm^{-1} due to water molecules together with a very weak sharp peak at 3650 cm^{-1} corresponding to hydroxyls. The H-O-H bending vibrations are represented by a peak at 1690 cm^{-1} together with a shoulder at 1630 cm^{-1}. By analogy with the IR spectrum for crandallite (Frost et al., 2011), with the same topology of PO_4 tetrahedra, the symmetric P-O stretching modes are represented by a peak at 1015 cm^{-1} and a shoulder at 970 cm^{-1}, while a shoulder at 1100 cm^{-1} corresponds to an antisymmetric stretching mode. The IR spectrum for elliottite differs considerably from that for its dimorph, penriceite (Elliott et al., 2022). The latter does not exhibit a sharp O-H stretching vibration, has lower wavenumber H-O-H bending modes (1630 and 1660 cm^{-1}) and has a more complex envelope of P-O stretching vibrations with three antisymmetric stretching mode bands. The 1690 cm^{-1} band in elliottite is at an unusually high wavenumber for the H-O-H bending mode of water molecules. It either corresponds to very strongly H-bonded H_2O or is due to the H-O-H bending mode of H_3O^+.

Chemical composition

Crystals of elliottite in specimen G35026 (Fig. 4) and in the type specimen of angastonite, M45575, were analysed using wavelength-dispersive spectrometry on a JEOL JXA 8500F Hyperprobe operated at an accelerating voltage of 15 kV and a beam current of 2 nA. Aggregates of edge-on platelets were analysed and the beam was defocused to typically 5 μm to minimize beam damage. Analytical results are given in Table 1. For comparison, the analyses of the closely associated dimorph, penriceite, are also given in Table 1. There was insufficient material for direct determination of H_2O, so it was based upon the dimorphic relationship to penriceite together with the crystal structure results.

The empirical formulae based on 23 anions are:

G35026: $Na_{0.56}K_{0.40}Ca_{0.02}Mg_{1.79}Al_{2.27}P_{2.02}F_{4.33}H_{20.19}O_{18.67}$

M45575: $Na_{0.54}K_{0.24}Ca_{0.23}Mg_{1.53}Al_{2.57}P_{2.11}F_{3.37}H_{20.07}O_{19.63}$

The simplified formula is
$(Na, K, Ca)Mg(Al, Mg)_3(PO_4)_2(F,OH,H_2O)_6 \cdot 9H_2O$.

The ideal end-member formula is
$NaMgAl_3(PO_4)_2F_6 \cdot 9H_2O$, which requires Na_2O 5.22, MgO 6.78, Al_2O_3 25.7, P_2O_5 23.9, F 19.2, H_2O 27.3, -O=F -8.1, total 100 wt%.

X-ray crystallography

Numerous platelets of elliottite were checked for their single-crystal (SC) diffraction quality at the macromolecular beam line MX2 of the Australian Synchrotron. None of them were of suitable quality for a SC data collection due to

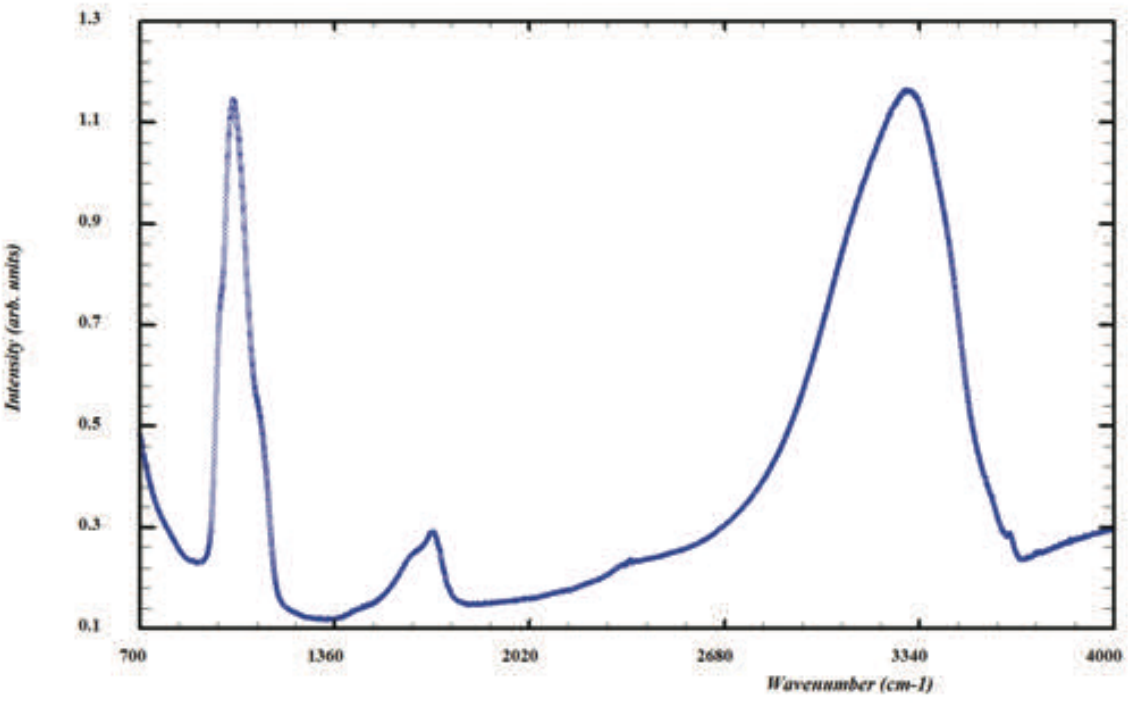

Figure 6 Infrared spectrum for elliottite, specimen G35026.

subparallel lamellae in the platelets giving peak splitting and streaking. However, the synchrotron study was able to confirm that the structure was based on a hexagonal (or pseudohexagonal) unit-cell base with a ~ 7.0 Å, and with spacing normal to the base of ~ 11 Å.

Platelet crystals of elliottite were ground and dispersed on a silicon disc for a powder X-ray diffraction (PXRD) data collect. A pattern was obtained at room temperature using a Panalytical Aeris diffractometer employing Co$K\alpha$ radiation. Step-scan data were collected in the two-theta range 5 to 80° using a step size of 0.022° and a step counting time of 1500 sec (6 h data collect). Elliottite was the dominant phase in the PXRD together with minor minyulite and a talc-like phase. Application of the indexing program DICVOL (Boultif and Louer, 2004) gave a *C*-centred monoclinic cell, with systematic absences consistent with *C*2/*m* or non-centrosymmetric subgroups *C*2 or *Cm*. LeBail profile refinement of the PXRD data using FULLPROF (Rodriguez-Carvajal, 1990) gave the unit-cell parameters: a = 12.242(1) Å, b = 7.0118(7) Å, c = 11.2946(9) Å, β = 101.19(1)°, with V = 951.1(2) Å^3 and Z = 2. Observed and calculated d values, intensities and indices are given in Table 2.

Table 1 Analytical data (wt%). Standard deviations given in parentheses.

Constituent	*G35026 (av. of 5)*	*M45575 (av. of 7)*	*Penriceite G32227 (av. of 7)*	*Standard*
Na_2O	2.93 (0.72)	2.83 (0.87)	4.39 (0.79)	Albite
K_2O	3.19 (0.25)	1.94 (0.54)	0.32 (0.29)	Adularite
CaO	0.21 (0.05)	2.22 (1.38)	1.58 (0.56)	Apatite
MgO	12.1 (0.8)	10.4 (1.9)	9.10 (0.86)	Spinel
Al_2O_3	19.4 (1.7)	22.1 (1.5)	22.7 (2.0)	Berlinite
P_2O_5	24.0 (1.1)	25.2 (2.3)	24.0 (1.7)	Berlinite
F	13.8 (1.2)	10.8 (1.4)	10.8 (1.1)	CaF_2
-O=F	-5.81	-4.56	-4.56	
H_2O	30.5	30.5	30.5	
Total	100.32	101.43	98.83	

Table 2 Powder X-ray diffraction data (d in Å) for elliottite

I_{obs}	d_{meas}	d_{calc}	h	k	l
100	11.076	11.080	0	0	1
9	6.059	6.055	1	1	0
12	5.782	5.768	-2	0	1
10	5.532	5.539	0	0	2
31	5.106	5.107	1	1	1
5	4.544	4.533	-2	0	2
3	3.506	3.506	0	2	0
6	3.346	3.342	0	2	1
3	3.196	3.197	-3	1	2
4	3.168	3.168	3	1	1
4	3.028	3.028	2	2	0
8	2.882	2.884	-4	0	2
17	2.852	2.850	2	2	1
3	2.765	2.770	0	0	4
		2.765	4	0	1
3	2.460	2.462	-2	2	3
3	2.447	2.448	4	0	2
2	1.951	1.952	3	3	1
		1.951	2	2	4
1	1.841	1.839	3	3	2
3	1.764	1.763	-6	2	1
2	1.754	1.753	0	4	0
1	1.711	1.710	2	2	5

Crystal structure

Based on the *C*-centred orthohexagonal unit-cell base, 7.0√3 x 7.0, and the evidence for a layer structure from textured PXRD patterns, a structural model for elliottite in space group *C*2/*m* was constructed containing crandallite-type layers of composition $[Al_3(PO_4)_2(F,OH)_6]^{3-}$. The layer coordinates for $Al_3(PO_4)_2(OH)_6$ from crandallite (Blount, 1974) were transformed into the monoclinic unit-cell for elliottite and the resulting calculated PXRD was found to give a good intensity match to the low-angle reflections. Fourier maps and difference-Fourier maps were used to locate the interlayer atoms and to slightly displace the layer anions (required because of minor substitution of Mg for Al in the octahedral sites).

The interlayer species were found to comprise dimers of edge-shared $Mg(H_2O)_6$ octahedra and water molecules, together with Na atoms occupying the centres of the hexagonal rings in the layers. The interlayer hydrated octahedra were found to be only half-occupied. Because of the partially occupied sites in the structure and the presence of minor impurity phases in the PXRD, refinement of atomic coordinates using the PXRD data was not attempted. The Rietveld refinement was restricted to profile parameters (unit cell parameters, peak shape, peak halfwidths), interlayer atom site-occupancies and an overall temperature factor. Minyulite was included as a minor impurity phase. The final Rietveld fit parameters were R_{wp} = 7.5, Ψ^2 = 5.2, R_{Bragg} = 8.2. The fitted Rietveld pattern is shown in Figure 7. The atomic coordinates are given in Table 3 and polyhedral bond distances are in Table 4.

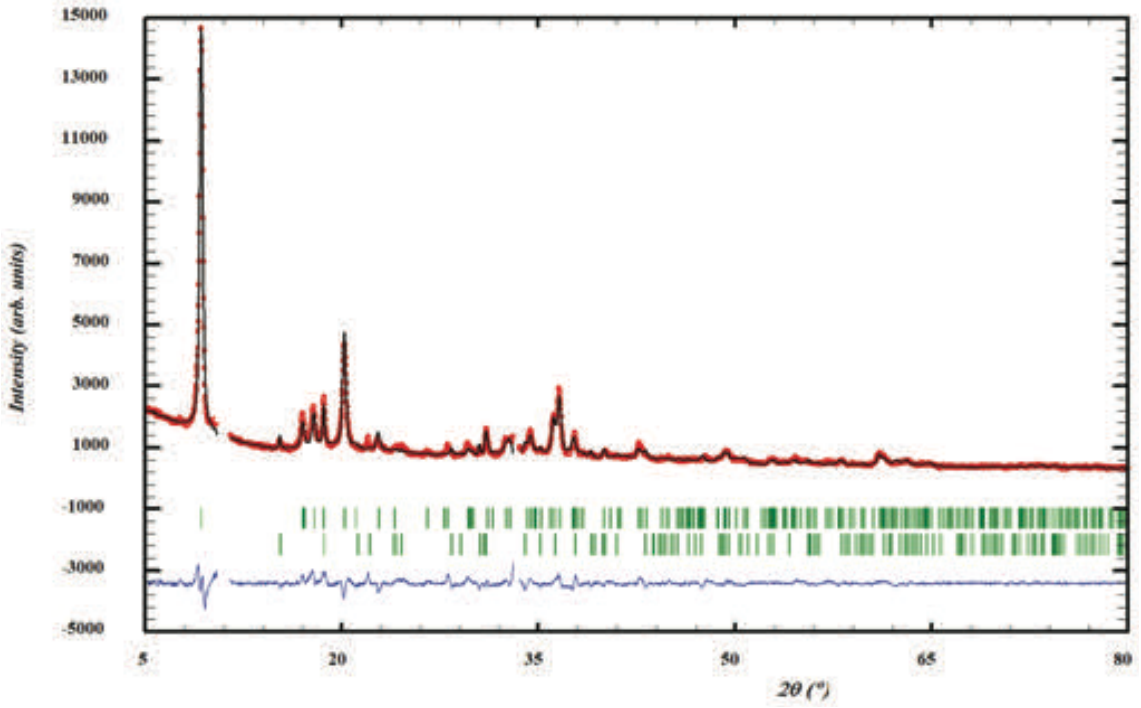

Figure 7 Rietveld fit to PXRD profile for elliottite. Upper tick marks are reflection positions for elliottite and lower tick marks are for minyulite impurity.

Table 3 Atom coordinates for elliottite

	Site	*Occ.*	*x*	*y*	*z*
Na	2*b*	0.68(3)	1/2	0	0
Mg	4*i*	0.522(7)	0.582	0	0.395
Al1	2*a*	1	0	0	0
Al2	4*e*	1	1/4	1/4	0
P	4*i*	1	0.871	0.0	0.209
O1	4*i*	1	0.892	0.0	0.348
O2	4*i*	1	0.981	0.0	0.164
O3	8*j*	1	0.802	0.177	0.162
F1	4*i*	1	0.686	0	0.0
F2	8*j*	1	0.891	0.200	0.958
Ow1	4*g*	0.522(7)	0	0.32	0.5
Ow2	4*i*	0.79(2)	0.58	0	0.71
Ow3	4*i*	1	0.74	0	0.5
Ow4	8*j*	1	0.40	0.19	0.75

Table 4 Polyhedral bond lengths [Å] for elliottite

Al1-O2 x2	1.911	Al2-O3 x2	1.888
Al1-F2 x4	1.930	Al2-F1 x2	1.976
Av.	1.924	Al2-F2 x2	1.909
		Av.	1.924
P-O1	1.546		
P-O2	1.529	Mg-Ow1 x2	2.11
P-O3 x2	1.537	Mg-Ow2	2.10
Av.	1.537	Mg-Ow3	2.06
		Mg-Ow4 x2	2.15
Na-O4 x2	2.48	Av.	2.11
Na-O5 x4	2.49		
Na-Ow4	3.15		
Av. (of 6)	2.487		

Discussion

A projection of the crystal structure of elliottite along [010] is shown in Figure 8a, where it is compared with the structure of penriceite (Fig. 8b), showing the different topology of the heteropolyhedral layers. In elliottite, the layers are built from planar nets of *trans*-corner-shared Al-centred octahedra decorated with PO_4 tetrahedra, whereas in penriceite, as in aldermanite (Elliott et al., 2021), the layers have a sawtooth shape and involve both *trans*- and *cis*-corner-sharing of octahedra. The structure of penriceite can be described in terms of periodic unit-cell-scale twinning of the elliottite structure. The relationship between the two structures is the same as that between the structures of the dimorphs orthoenstatite and clinoenstatite, where orthorhombic orthoenstatite structure has been described as unit-cell twinning of the monoclinic clinoenstatite structure (Morimoto and Koto, 1969).

In penriceite the sodium atoms at the centre of the 6-member rings have 8-coordinated scalenohedral coordination whereas in elliottite the sodium is 6-coordinated as a very flat octahedron. In penriceite the interlayer $Mg(H_2O)_6$ octahedra are isolated whereas in elliottite they share edges, giving $Mg_2(H_2O)_{10}$ dimers. Penriceite has a much larger layer spacing (13.5 Å), resulting in a quite different PXRD pattern to that for elliottite with a 11.1 Å layer spacing. The properties of elliottite and penriceite are compared in Table 5.

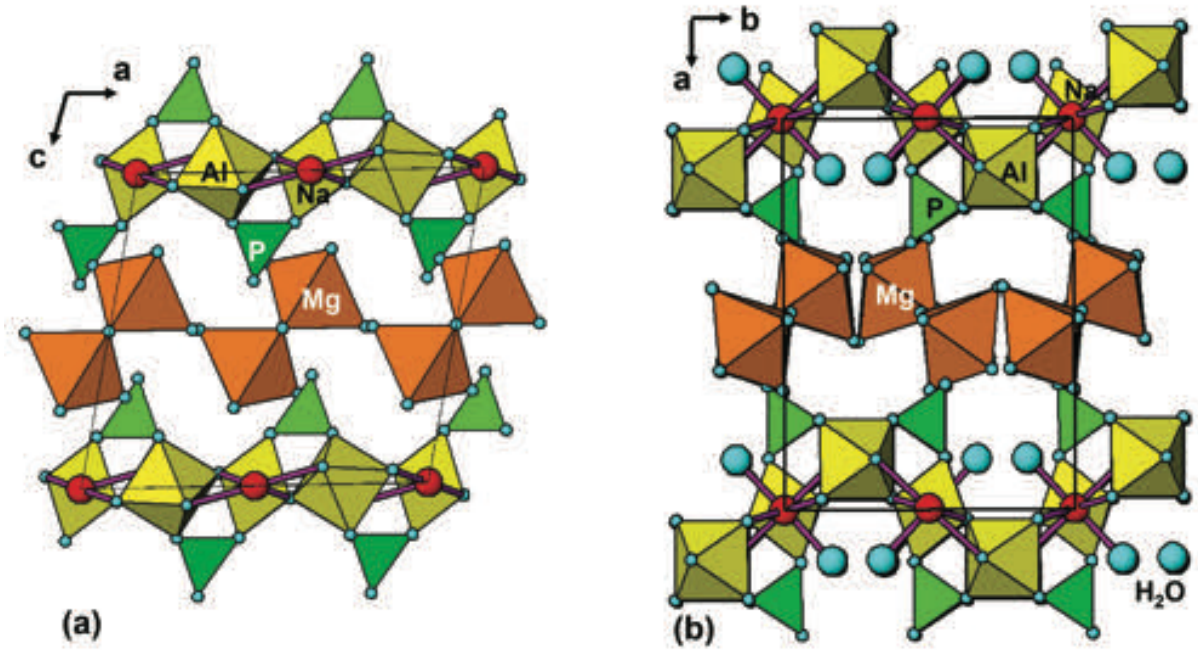

Figure 8 **(a) [010] projection of the structure of elliottite and (b) [001] projection of the structure of penriceite.**

Table 5 **Comparison of properties for elliottite and penriceite**

	Elliottite	*Penriceite*
Ideal formula	$NaMgAl_3(PO_4)_2F_6{\cdot}9H_2O$	$[Mg(H_2O)_6][Na(H_2O)_2Al_3(PO_4)_2F_6]{\cdot}H_2O$
Symmetry	Monoclinic, *C*2/*m*	Monoclinic, $P2_1/c$
a (Å)	12.2420(10)	13.478(3)
b (Å)	7.0118(7)	9.971(2)
c (Å)	11.2946(9)	6.9990(10)
β (°)	101.19(1)	97.20(3)
Volume (Å^3), *Z*	951.1(2), 2	933.2(3), 2
Optics	Biaxial (+), α = β = 1.475(2)	Biaxial (+), α = 1.502(2)
	γ = 1.479(2)	β = 1.503(2), γ = n.d.
Strongest lines in PXRD	11.08, 100 (001)	13.39, 100 (100)
d, *I* (*hkl*)	6.059, 9 (110)	8.000, 30 (110)
	5.782, 12 (-201)	5.562, 26 (210)
	5.106, 31 (111)	5.718, 12 (011)
	2.882, 8 (-402)	2.855, 16 (022)
	2.852, 17 (221)	2.782, 15 (420)

Acknowledgments

The infrared spectrum was acquired with the assistance of the Forensic Science Centre, Adelaide. We acknowledge the Diffraction Laboratory at CSIRO Mineral Resources, Clayton, for use of their Panalytical Empyrean powder XRD diffractometer. Thanks to Cameron Davidson and Matt Glenn for EMP sample preparation and for SEM images. Thanks to Peter Downes for redrafting the map and to Allan Pring for reviewing the manuscript.

References

Blount AM, 1974. The crystal structure of crandallite: *American Mineralogist*, v. 59, p. 41–47.

Boultif A and Louer D, 2004. Program for the automatic indexing of powder diffraction patterns by the successive dichotomy method. *Journal of Applied Crystallography*, v. 37, p. 724–731.

Elliott P, 2016. Jahnsite-(CaFeMg), a new mineral from Tom's quarry, South Australia: description and crystal structure: *European Journal of Mineralogy*, v. 28, p. 991–996.

Elliott P, Grey IE, MacRae CM, Kampf AR and Davidson C, 2022. Penriceite $[Mg(H_2O)_6][Na(H_2O)Al_3(PO_4)F_6]\cdot H_2O$, the F-analogue of aldermanite, from the Penrice marble quarry, South Australia: *Australian Journal of Mineralogy,* v. 23(1), p. 5–12.

Elliott P, Grey IE and Willis AC, 2021. Redefinition of the formula for aldermanite, $[Mg(H_2O)_6][Na(H_2O)_2Al_3(PO_4)_2(OH,F)_6]\cdot H_2O$, and its crystal structure: *Mineralogical Magazine*, v. 85, p. 348–353.

Elliott P, Peisley V and Mills SJ, 2013. The phosphate deposits of South Australia: *Australian Journal of Mineralogy*, v. 17, p. 3–32.

Frost R, Xi Y, Palmer S and Pogson R, 2011. Vibrational spectroscopic analysis of the mineral crandallite $CaAl_3(PO_4)_2(OH)_5\cdot(H_2O)$ from the Jenolan caves, Australia: *Spectrochimica Acta Part A: Molecular and Biomolecular Spectroscopy*, v. 82, p. 461–466.

Grey IE, Elliott P, Mumme WG, MacRae CM, Kampf AR and Mills SJ, 2022a. Redefinition of angastonite, $CaMgAl_2(PO_4)_2(OH)_4\cdot 7H_2O$, as an amorphous mineral: *European Journal of Mineralogy*, v. 34, p. 215–221.

Grey IE, MacRae CM, Elliott P, Mills S and Downes PJ, 2022b. Minyulite, $KAl_2F(PO_4)_2\cdot 4H_2O$: Approval of revised formula and its stability in South Australian rock phosphate deposits: *Australian Journal of Mineralogy,* v. 23(1), p. 21–25.

Mandarino JA, 1981. The Gladstone-Dale relationship: Part IV. The compatibility concept and its application: *Canadian Mineralogist*, v. 19, p. 441–450.

Mills SJ, Birch WD, Kampf AR, Christy AG, Pluth JJ, Pring A, Raudsepp M and Chen Yu-S, 2010. Kapundaite, a new phosphate species from Tom's quarry, South Australia: description and structural relationship to melonjosephite: *American Mineralogist*, v. 95, p. 754–760.

Mills SJ, Groat LA, Wilson SA, Birch WD, Whitfield PS and Raudsep M, 2008. Angastonite, $CaMgAl_2(PO_4)_2(OH)_4\cdot 7H_2O$: a new phosphate mineral from Angaston, South Australia: *Mineralogical Magazine*, v. 72, p. 1011–1020.

Mills SJ, Ma C and Birch WD, 2011. A contribution to understanding the complex nature of peisleyite: *Mineralogical Magazine*, v. 75, p. 2733–2737.

Morimoto N and Koto K, 1969. The crystal structure of orthoenstatite: *Zeitschrift fur Kristallographie*, v. 129(8), p. 65–83.

Pilkington ES, Segnit ER and Watts JA, 1982. Peisleyite, a new sodium aluminium sulphate phosphate: *Mineralogical Magazine*, v. 46, p. 449–452.

Rodriguez-Carvajal J, 1990. FULLPROF: A Program for Rietveld refinement and Pattern Matching Analysis: Satellite meeting on powder diffraction of the Fifteenth General Assembly and International Congress of Crystallography, Toulouse, France. 16–19 July, 1990.